Supplementary information for

High-throughput development of tough metallic glass films

Yuzhou Wu,[ab‡] Yue Huang,[ab‡] Yebei Wang,[a‡] Fuchao Wang,[a] Yunhe Gao,[a] Yingying Sun,[a] Meichen Jian,[a] Lijian Song,[a] Yu Tong,[a] Yan Zhang,[a] Chao Wang,[c] Yanhui Liu,[c] Jun-Qiang Wang,[*a] Juntao Huo,[*a] Meng Gao[*a]

[a] *Ningbo Institute of Materials Technology and Engineering, Chinese Academy of Sciences, Ningbo 315201, China.*

[b] *School of Materials Science and Chemical Engineering, Ningbo University, Ningbo 315211, China.*

[c] *Institute of Physics, Chinese Academy of Sciences, Beijing 100190, China.*

[*] Corresponding authors.

E-*mail addresses*: gaomeng@nimte.ac.cn (M. Gao), huojuntao@nimte.ac.cn (J.T. Huo), jqwang@nimte.ac.cn (J.Q. Wang).

[‡] These authors contributed equally to this work.

This supplementary information file includes:

- Fig. S1. Three-dimensional AFM surface topography corresponding to one amplified local region in Fig. 1b marked by red dotted circle.
- Fig. S2. The detailed nanoindentation load and displacement curves with different nanoindentation depths h_m for $Zr_{38}Ti_{10}Cu_{29}Al_{23}$ MGF.
- Fig. S3. The toughness values at different indentation depths for $Zr_{38}Ti_{10}Cu_{29}Al_{23}$ MGF.
- Fig. S4. Comparison of the values of measured toughness by the nanoindentation energy conversion method and the traditional three-point bending methods for $Zr_{61}Ti_2Cu_{25}Al_{12}$ bulk MG.
- Fig. S5. Structural characterizations for sample 1 (a, b, c), sample 2 (d, e, f) and sample 3 (g, h, i). HRTEM images and the corresponding electron diffraction patterns are shown in a, d, g. Dimple fracture structures characterized by SEM are shown in b, e, h, and the corresponding statistical analyses of the size of dimple structures are shown in c, f, i.
- Fig. S6. Correlation between EWF and toughness for various metals and alloys.
- Fig. S7. The composition mapping images of the HRTEM image for sample 1. Different images correspond to different compositions in the same location: Al (b), Cu (c), Zr (d), Ti (e), and O (f).
- Fig. S8. The chemical composition distribution of Zr, Ti, Cu, and Al elements in the second sample library.
- Fig. S9. The XRD patterns of three kinds of flexible films deposited by magnetron co-sputtering, all of which are amorphous.
- Fig. S10. Comparison of toughness for MGFs deposited on different substrates: single-crystal silicon (blue point) and PET (red point).
- Table S1. The proportions of each chemical element for sample 1, 2, and 3 with single crystal silicon substrate by EDS.
- Table S2. The proportions of each chemical element for sample 1, 2, 3 with single crystal silicon substrate and sample 1, 2, 3 with PET substrate by XPS.

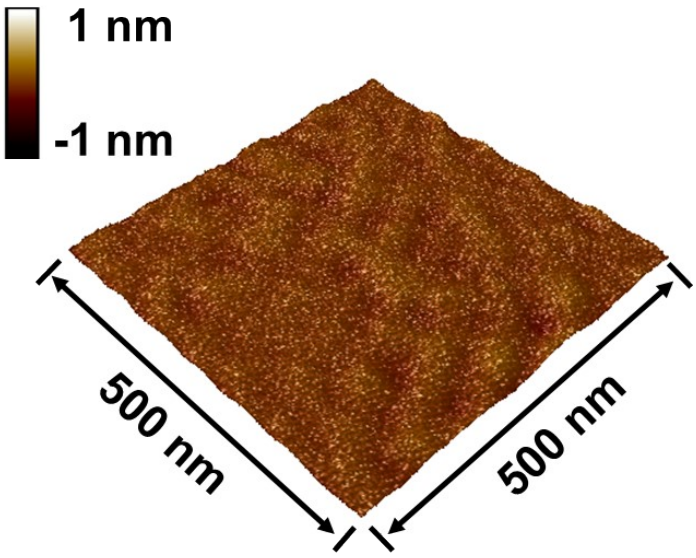

Fig. S1 Three-dimensional AFM surface topography corresponding to one amplified local region in Fig. 1b marked by red dotted circle.

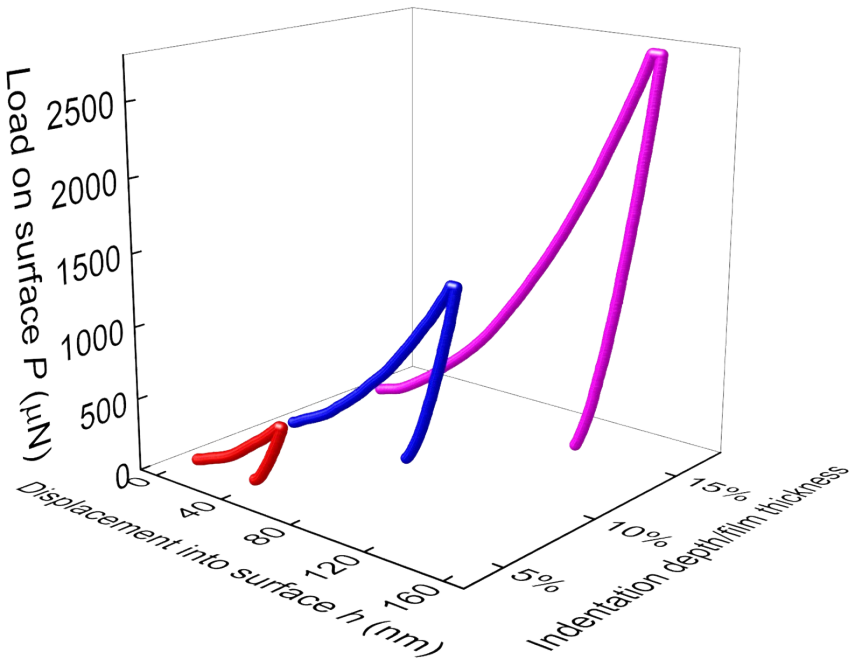

Fig. S2 The detailed nanoindentation load and displacement curves with different nanoindentation depths h_m for $Zr_{38}Ti_{10}Cu_{29}Al_{23}$ MGF.

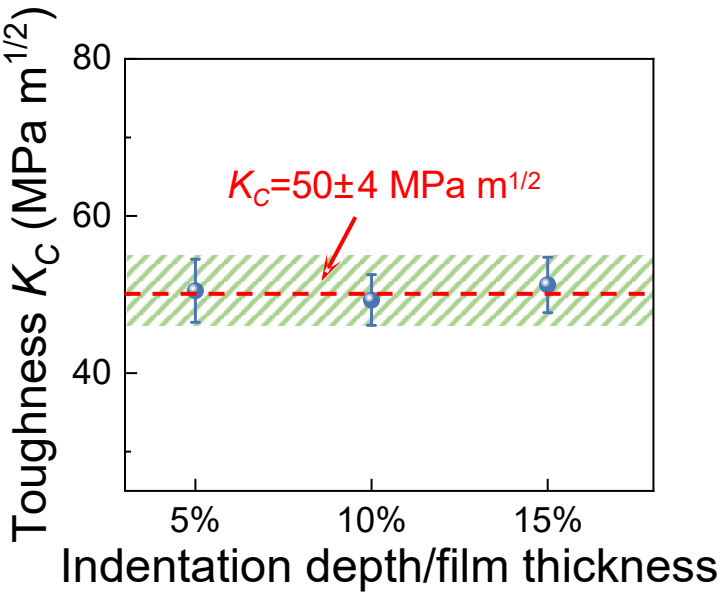

Fig. S3 The toughness values at different indentation depths for $Zr_{38}Ti_{10}Cu_{29}Al_{23}$ MGF.

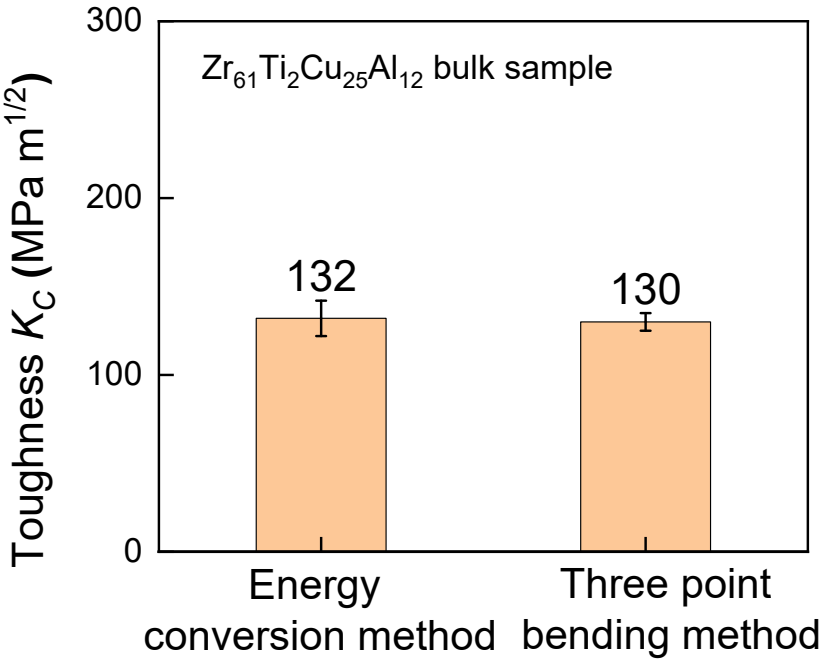

Fig. S4 Comparison of the values of measured toughness by the nanoindentation energy conversion method and the traditional three-point bending methods for $Zr_{61}Ti_2Cu_{25}Al_{12}$ bulk MG.

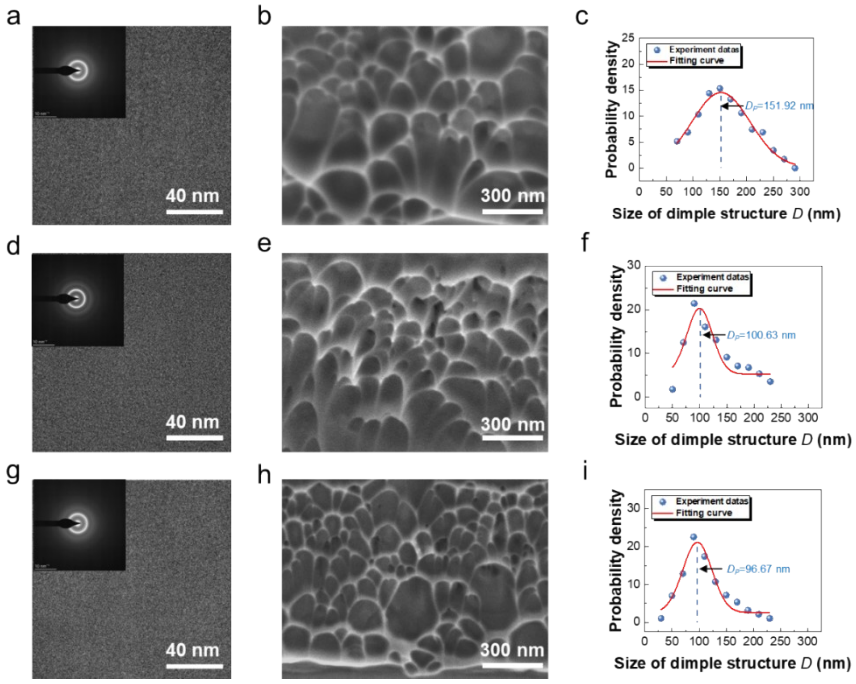

Fig. S5 Structural characterizations for sample 1 (a, b, c), sample 2 (d, e, f) and sample 3 (g, h, i). HRTEM images and the corresponding electron diffraction patterns are shown in a, d, g. Dimple fracture structures characterized by SEM are shown in b, e, h, and the corresponding statistical analyses of the size of dimple structures are shown in c, f, i.

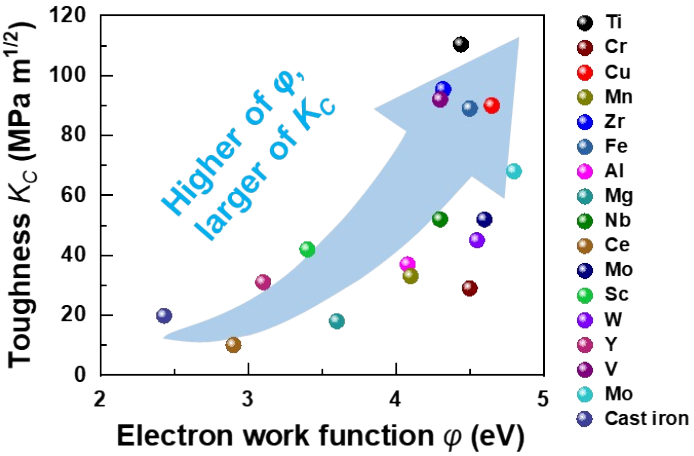

Fig. S6 Correlation between EWF and toughness for various metals and alloys.

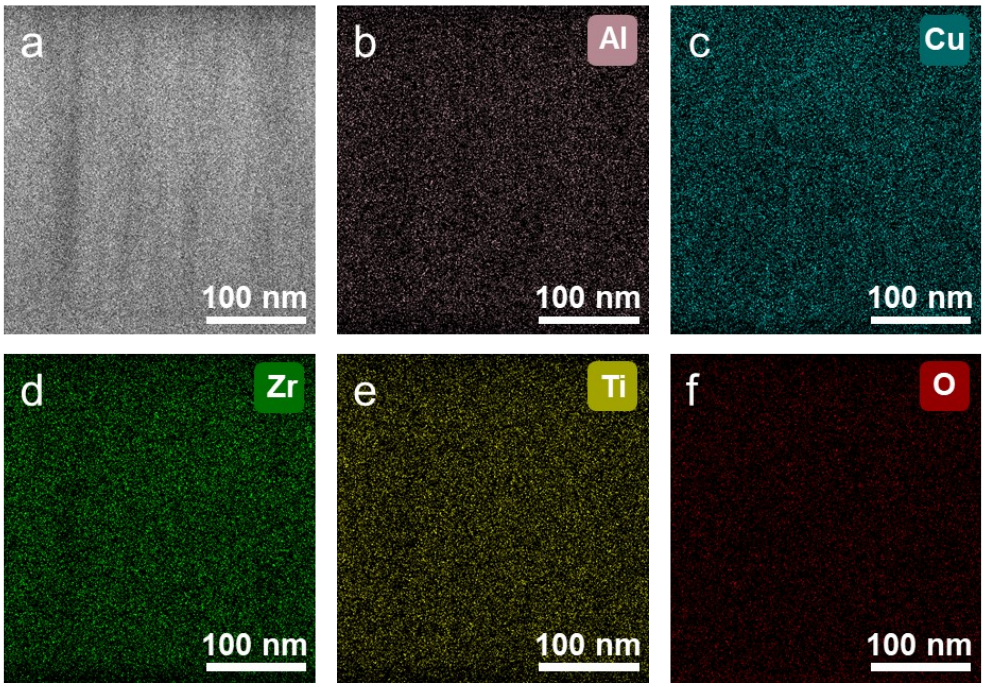

Fig. S7 The composition mapping images of the HRTEM image for sample 1. Different images correspond to different compositions in the same location: Al (b), Cu (c), Zr (d), Ti (e), and O (f).

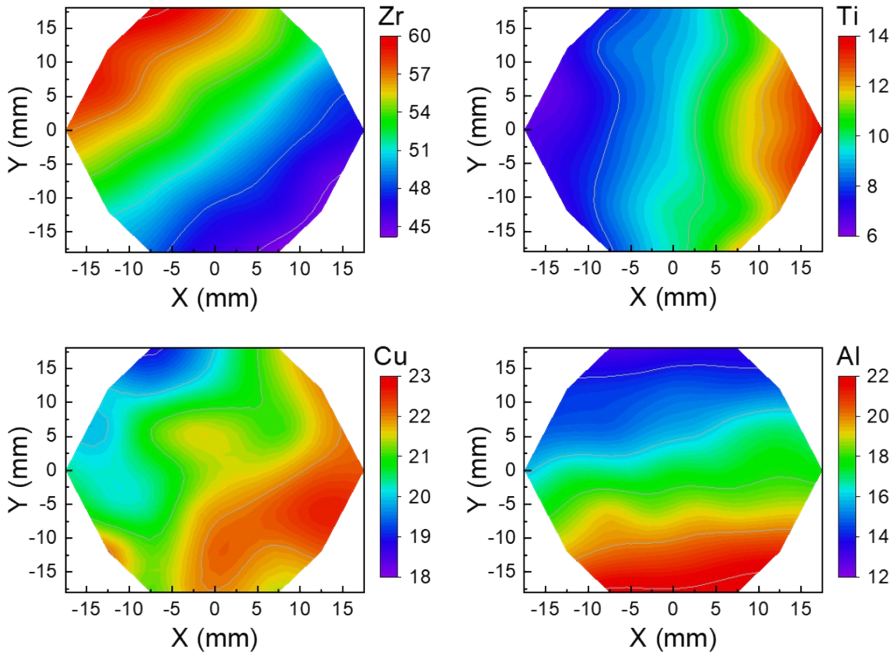

Fig. S8 The chemical composition distribution of Zr, Ti, Cu, and Al elements in the second sample library.

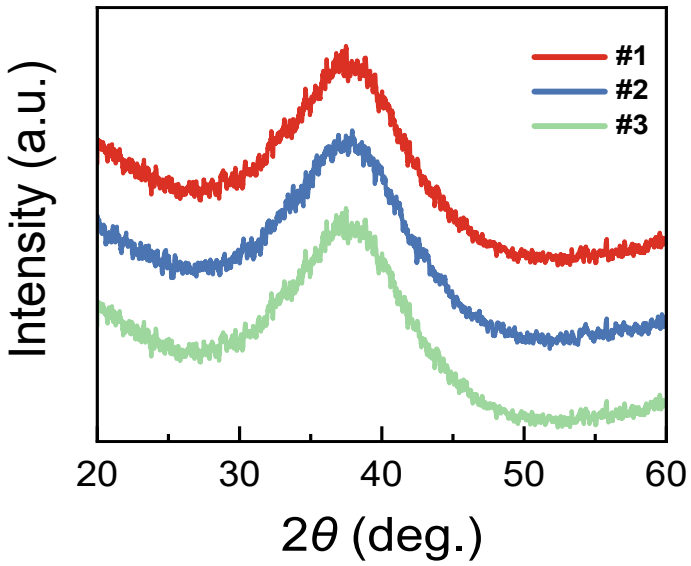

Fig. S9 The XRD patterns of three selected MGF samples with different toughnesses deposited by magnetron co-sputtering.

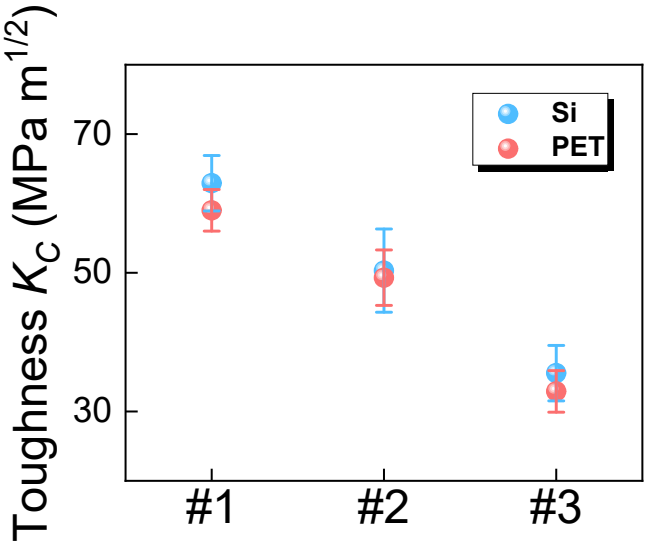

Fig. S10 Comparison of toughness for MGFs deposited on different substrates: single-crystal silicon (blue point) and PET (red point).

Table S1. The proportions of each chemical element for sample 1, 2, and 3 with single crystal silicon substrate by EDS.

Sample	Percent of Zr (%)	Percent of Ti (%)	Percent of Cu (%)	Percent of Al (%)	Percent of O (%)
Sample 1-Si	38.05	9.50	28.65	22.53	1.27
Sample 2-Si	48.03	7.58	26.69	16.53	1.17
Sample 3-Si	60.54	1.76	24.69	11.60	1.41

Table S2. The proportions of each chemical element for sample 1, 2, 3 with single crystal silicon substrate and sample 1, 2, 3 with PET substrate by XPS.

Sample	Percent of Zr (%)	Percent of Ti (%)	Percent of Cu (%)	Percent of Al (%)	Percent of O (%)
Sample 1-Si	37.56	9.82	28.74	22.72	1.16
Sample 2-Si	47.72	7.81	26.52	16.74	1.21
Sample 3-Si	60.65	1.75	24.77	11.75	1.08
Sample 1-PET	37.91	9.75	28.55	22.66	1.13
Sample 2-PET	48.04	7.65	26.59	16.62	1.10
Sample 3-PET	60.76	1.83	24.64	11.54	1.23